minerals

MDPI

Article

A NanoSIMS 50 L Investigation into Improving the Precision and Accuracy of the $^{235}U/^{238}U$ Ratio Determination by Using the Molecular $^{235}U^{16}O$ and $^{238}U^{16}O$ Secondary Ions

N. Alex Zirakparvar *, Cole R. Hexel, Andrew J. Miskowiec, Julie B. Smith, Michael W. Ambrogio, Douglas C. Duckworth, Roger Kapsimalis and Brian W. Ticknor

Oak Ridge National Laboratory, 1 Bethel Valley Rd, Oak Ridge, TN 37830, USA; hexelcr@ornl.gov (C.R.H.); miskowiecaj@ornl.gov (A.J.M.); smithjb1@ornl.gov (J.B.S.); ambrogiomw@ornl.gov (M.W.A.); duckworthdc@ornl.gov (D.C.D.); kapsimalisrj@ornl.gov (R.K.); ticknorbw@ornl.gov (B.W.T.)

* Correspondence: zirakparvana@ornl.gov; Tel.: +1-(347)6-864-146

Received: 19 February 2019; Accepted: 15 May 2019; Published: 18 May 2019

Abstract: A NanoSIMS 50 L was used to study the relationship between the $^{235}U/^{238}U$ atomic and $^{235}U^{16}O/^{238}U^{16}O$ molecular uranium isotope ratios determined from a variety of uranium compounds (UO_2, UO_2F_2, UO_3, $UO_2(NO_3)_2{\cdot}6(H_2O)$, and UF_4) and silicates (NIST-610 glass and the Plesovice zircon reference materials, both containing μg/g uranium). Because there is typically a greater abundance of $^{235}U^{16}O^+$ and $^{238}U^{16}O^+$ molecular secondary ions than $^{235}U^+$ and $^{238}U^+$ atomic ions when uranium-bearing materials are sputtered with an oxygen primary ion beam, the goal was to understand whether use of $^{235}U^{16}O/^{238}U^{16}O$ has the potential for improved accuracy and precision when compared to the $^{235}U/^{238}U$ ratio. The UO_2 and silicate reference materials showed the greatest potential for improved accuracy and precision through use of the $^{235}U^{16}O/^{238}U^{16}O$ ratio as compared to the $^{235}U/^{238}U$ ratio. For the UO_2, which was investigated at a variety of primary beam currents, and the silicate reference materials, which were only investigated using a single primary beam current, this improvement was especially pronounced at low $^{235}U^+$ count rates. In contrast, comparison of the $^{235}U^{16}O/^{238}U^{16}O$ ratio versus the $^{235}U/^{238}U$ ratio from the other uranium compounds clearly indicates that the $^{235}U^{16}O/^{238}U^{16}O$ ratio results in worse precision and accuracy. This behavior is based on the observation that the atomic ($^{235}U^+$ and $^{238}U^+$) to molecular ($^{235}U^{16}O^+$ and $^{238}U^{16}O^+$) secondary ion production rates remain internally consistent within the UO_2 and silicate reference materials, whereas it is highly variable in the other uranium compounds. Efforts to understand the origin of this behavior suggest that irregular sample surface topography, and/or molecular interferences arising from the manner in which the UO_2F_2, UO_3, $UO_2(NO_3)_2{\cdot}6(H_2O)$, and UF_4 were prepared, may be a major contributing factor to the inconsistent relationship between the observed atomic and molecular secondary ion yields. Overall, the results suggest that for certain bulk compositions, use of the $^{235}U^{16}O/^{238}U^{16}O$ may be a viable approach to improving the precision and accuracy in situations where a relatively low $^{235}U^+$ count rate is expected.

Keywords: NanoSIMS; uranium; isotope ratio mass spectrometry; secondary ion; matrix effect

1. Introduction

The use of SIMS (secondary ion mass spectrometry) to determine the $^{235}U/^{238}U$ isotope ratio of environmental uranium microparticles was first reported in [1]. Since then, SIMS has become a routine technique for determining the $^{235}U/^{238}U$ and other isotope ratios of uranium compounds, both on individual particles and on bulk materials (up-to-date summaries can be found in [2–6]).

As with any isotope ratio determination, internal precision of the $^{235}U/^{238}U$ ratio determined by SIMS is strongly associated with the count rate of the minor isotope (e.g., [7]). For isotope measurements focused on determination of the $^{235}U/^{238}U$ ratio from depleted/natural uranium, this is always the ^{235}U. The magnitude of deviance (relative to the 'true' values) and internal precision exhibited by reference materials, as well as the robustness of mass fractionation correction regimes, are also typically factored into the determination of the total uncertainty associated with individual measurements of the 'unknowns' (see discussion by [8]). For SIMS analysis, additional issues are associated with the matrix effect, which refers to the long-recognized phenomenon (e.g., [9]) that secondary ion production rates vary widely between different materials for the same ion, and between different elements. These issues have been investigated for the determination of $^{235}U/^{238}U$ from uranium compounds by SIMS in several studies (e.g., [5,10,11]), but these investigations have mostly focused on the use of the large and small geometry (LG- and SG-, respectively) SIMS instruments (e.g., the Cameca® IMS-1280 and 7f imf series).

More recently, Cameca® has developed the NanoSIMS platform (described in [12]), which blends aspects of the LG-SIMS (e.g., high sensitivity and mass resolving power [MRP], defined as M/ΔM at 10% peak height) with redesigned ion optics that allow for a significant reduction in the size of the primary beam impinging on the sample surface (aka. 'beam footprint'). However, this reduction in primary beam footprint comes with a reduction in the primary beam current. For example, NanoSIMS analyses are typically conducted using primary currents up to a few hundred picoamps (pA), whereas other SIMS instruments typically operate with beam currents >5 nanoamps (nA). The significantly smaller primary beam footprint that is achievable on the NanoSIMS can enable the resolution of smaller features compared to the other SIMS instruments, but the lower beam currents needed to achieve this higher spatial resolution result in reduced secondary ion count rates. The fact that lower primary beam currents equate to a smaller mass of total sputtered material could be advantageous in situations where there is a need to preserve as much of the material as possible and/or regions of interest are sub-micron; however, a caveat is that lower secondary ion count rates can result in increased analytical uncertainty (see discussion by [10]).

This increase in uncertainty at low count rates is especially evident when the target analyte is present as a trace constituent of the material in question (e.g., uranium present at parts per million [ppm] levels in a silicate or metallic bulk matrix), there is a small quantity of the material available (e.g., single particle analysis), the minor isotope of the desired ratio is present at considerably lower levels compared to the major isotope (e.g., uranium compounds with natural to depleted $^{235}U/^{238}U$ ratios), or a combination of these factors. Therefore, there are a relatively limited number of approaches that can be taken to improve the number of secondary ions available for detection, which is a key necessity for improving precision and accuracy in count-rate-limited situations. A higher primary beam current could be used, or the transmission through the instrument could be increased. However, this would result in a drop in spatial resolution, an increase in the amount of material being consumed, a decrease in MRP resulting from increased transmission through the instrument, or a combination of these effects.

When a material is sputtered during SIMS analysis, single element atomic ions as well as multi-element molecular ions are produced (see discussion by [13]). In situations where the material being sputtered contains an abundance of oxygen, or an oxygen ion primary beam is used, atomic elemental ions (e.g., $^{235}U^+$ and $^{238}U^+$) and their molecular elemental oxide ions ($^{235}U^{16}O^+$, $^{238}U^{16}O^+$) are produced. In the case of uranium analysis, which is typically performed using an oxygen ion primary beam because uranium does not ionize well under other commonly available ion beams (e.g., Cs^+; see discussion by [14]), there is often a greater abundance of molecular uranium oxide ($^{235}U^{16}O^+$ and $^{238}U^{16}O^+$) compared to atomic elemental ($^{235}U^+$ and $^{238}U^+$) secondary ions recorded on the detectors. This phenomenon is especially well documented in the field of SIMS U-Pb zircon geochronology (see discussion by [15]). Specific to the NanoSIMS, $^{238}U^{16}O^+$ molecular secondary ions are typically five times more abundant than $^{238}U^+$ atomic ions when zircon containing trace levels of uranium is sputtered with an O^- primary ion beam (refer to Figure 8 in [16]).

Determination of the $^{235}U/^{238}U$ ratio from uranium compounds by SIMS has typically focused on use of the atomic ^{235}U and ^{238}U secondary ions (refer to [6] for a comprehensive summary of actinide analysis by SIMS). While use of the molecular $^{235}U^{16}O_2$ and $^{238}U^{16}O_2$ secondary ion species has been shown [3] to be a viable means of mitigating metallic molecular isobaric interferences on ^{235}U and ^{238}U for SIMS instruments with relatively low MRP, use of the molecular uranium secondary ions has not yet been systematically investigated in SIMS instruments capable of achieving high enough MRP values (e.g., the LG-SIMS instruments) to separate some of the more common molecular isobars (see discussion in [3]) that interfere with the monoatomic ^{235}U and ^{238}U. Because certain molecular isobars can be mitigated at high MRP, the primary mechanisms for improved precision and accuracy would be improved count rate by using molecular uranium oxides species ($^{235}U^{16}O^+$ and $^{238}U^{16}O^+$) in comparison to the atomic $^{235}U^+$ and $^{238}U^+$ species.

If the NanoSIMS is to be increasingly used for determining the $^{235}U/^{238}U$ ratio, it is worthwhile to investigate whether use of the $^{235}U^{16}O/^{238}U^{16}O$ molecular secondary ion ratio can provide better internal precision (as reflected by the degree of scatter associated with the individual cycles comprising a single measurement) and accuracy (as reflected by the deviance, relative to the 'true' value for a given material, of the $^{235}U/^{238}U$ and $^{235}U^{16}O/^{238}U^{16}O$ ratios calculated by averaging the individual cycles comprising each measurement together) compared to the $^{235}U/^{238}U$ ratio. As previously mentioned, there are many sources of uncertainty and a variety of correction regimes that can be factored into the reporting of a final isotope ratio; however, a first principle is that a raw measurement displaying good precision and accuracy will produce a higher-quality final result compared to a raw measurement with low precision that deviates strongly from the 'true' value, or both.

This study shows that the $^{235}U^{16}O/^{238}U^{16}O$ molecular secondary ion ratio can improve the internal precision and accuracy for certain uranium bulk matrices, whereas for other uranium bulk matrices it results in no discernable improvement. Furthermore, for a few of the uranium bulk matrices examined, use of the $^{235}U^{16}O/^{238}U^{16}O$ ratio is associated with an order of magnitude reduction in internal precision and accuracy of the raw measurement as compared to $^{235}U/^{238}U$ ratio. This conclusion is achieved by comparison of the $^{235}U/^{238}U$ atomic and $^{235}U^{16}O/^{238}U^{16}O$ molecular secondary ion ratios acquired on the NanoSIMS with $^{235}U/^{238}U$ values determined by solution multi-collector inductively coupled plasma mass spectrometry (MC-ICP-MS; for the uranium compounds) and reported in the literature (for the silicate reference materials). The possible causes of this inconsistent behavior are discussed in terms of the SIMS matrix effect, carbon- and fluorine-based molecular interferences, as well as other factors known to influence the sputtering and ionization process.

2. Materials and Methods

2.1. Materials

Materials analyzed in this study: A variety of uranium compounds, all produced at Oak Ridge National Laboratory [17–20], (UO_2, UO_2F_2, UO_3, $UO_2(NO_3)_2{\cdot}6(H_2O)$, and UF_4) as well as two silicate reference materials of known uranium isotope composition (the NIST-610 glass as well as the Plesovice zircon [17]). The NIST-610 glass and Plesovice zircons are widely used reference materials in the geosciences. Specific to this study, the uranium isotopic composition of the NIST-610 glass is $^{235}U/^{238}U = 0.0023956 \pm 0.0000005$, determined by [21]. The uranium concentration of the Plesovice zircon is described in [22], and the zircon is assumed to a have a natural $^{235}U/^{238}U$ ratio of 0.0072549 ± 0.0000008, which is the consensus value reported in [23].

The UO_2 material used was a ≥150 µm diameter sphere that was prepared from UO_3 synthesized via an internal gelation route described in [17]. The UO_3 microspheres, which were not the UO_3 that was analyzed in this study, were reduced to UO_2 by calcination and sintering for 5 h at 600 °C and 3 h at 1700 °C under a reducing atmosphere (Ar—4% H_2). The UO_2F_2 was produced by hydrolysis of UF_6 in a controlled atmosphere environment. UF_6 was released into a chamber at approximately 23% relative humidity at 24 °C. Particulate UO_2F_2 was collected on vinyl collection surfaces. The matter

was calcined overnight under a stream of 10 mL/s N_2 gas at 150 °C, which has previously been shown to produce anhydrous uranyl fluoride [18].

The UO_3 analyzed in this study was prepared by heating $UO_2(NO_3)_2{\cdot}6(H_2O)$ in air at 225 °C for 12 h, producing an amorphous uranium oxide, but no additional steps were taken to remove residual nitrogen after calcination. The UF_4 was produced by reducing UF_6 in NO_x in a two-step process (see [19,20]). First, $NOUF_6$ (nitrosylium hexafluorouranate) was produced by exposing frozen UF_6 to liquid N_2O_4. The $NOUF_6$ was then converted to UF_4 by devolatilizing NO_x compounds at 350 °C for 120 min in the presence of H_2 gas. No additional information is available about the origin of the $UO_2(NO_3)_2{\cdot}6(H_2O)$. Raman analysis of the materials on the mount containing the uranium compounds was performed to confirm their bulk chemistry.

2.2. Sample Preparation for NanoSIMS Analysis

For NanoSIMS analysis, the materials described above were potted in epoxy resin (Buehler EpoThin2). Two mounts were made. One mount contained all the uranium compounds (UO_2, UO_2F_2, UO_3, $UO_2(NO_3)_2{\cdot}6(H_2O)$, and UF_4), whereas the other contained the NIST-610 glass and the Plesovice zircon reference material. After allowing the epoxy to cure for approximately 1 week under ambient conditions, the mounts were ground and polished using successively finer silicon carbide-based abrasives, with a final polishing step using 0.25 µm diamond paste. An important difference between the two mounts was that the uranium compounds were polished using mineral oil as a lubricant, whereas the mount containing the NIST-610 glass and Plesovice zircon were polished in water. Mineral oil lubricant was selected for the uranium compounds because of the solubility of uranyl fluoride and uranyl nitrate in water. Methyl alcohol and acetone were used as cleaning agents for both mounts. Following a final cleaning step, and immediately before introduction into NanoSIMS airlock system, both mounts were coated with 100 nm of gold using a Cressington® 208 HR sputter coater outfitted with an MTM-20 thickness controller.

Representative scanning electron microscope (SEM) images, collected using a Zeiss® Merlin™ field-emission SEM, of two (the UO_2 and UO_2F_2) of the uranium compounds are provided in Figure 1. Images were initially collected using a secondary electron detector with an accelerating voltage of 10.0 kV and a beam current of 1.1 nA. The high-resolution images displayed in Figure 1 were then collected using an in-column detector, with an accelerating voltage of 1.5 kV and a beam current of 80 pA. There are two images for each of the uranium compounds shown. In the left panel, a relatively wide field of view is shown, whereas in the right panel, a close-up image of NanoSIMS analytical craters made using a static 200 pA primary beam (see Section 2.3 for further details pertaining to NanoSIMS analysis) is provided. It is important to note, however, that these craters were made as part of a series of experiments that preceded the isotope ratio measurements detailed in this study. Following acquisition of the images shown in Figure 1, the mount was repolished and recoated with 100 nm of gold before being introduced back into the NanoSIMS for the analyses described in this paper. However, the pit geometries and material surfaces should be representative of the data acquired in this study because the same 200 pA primary beam conditions were used, and the material preparation steps were identical. Immediately following the NanoSIMS isotope data acquisition reported in this study, the mount containing the uranium compounds was removed from the instrument. A portion of the uranium materials were then excavated from the mount for solution isotope analysis (see Section 2.4).

Following the sample processing and characterization procedure described, and in order to specifically assess questions over the role of sample preparation on the $^{235}U/^{238}U$ vs. $^{235}U^{16}O/^{238}U^{16}O$ ratios that arose during data interpretation, UO_2 taken from the same batch described in Section 2.1 was mounted in epoxy using the preparation described above, crushed in an agate mortar and then dispersed onto a sticky carbon tab (9 mm Leit® tabs), as well as pressed into high purity Indium metal. Prior to analysis (in their own session; see Section 2.3) on the NanoSIMS, the UO_2 mounted in epoxy and pressed into Indium were coated with 100 nm Au, whereas the UO_2 dispersed onto the sticky carbon tab was not.

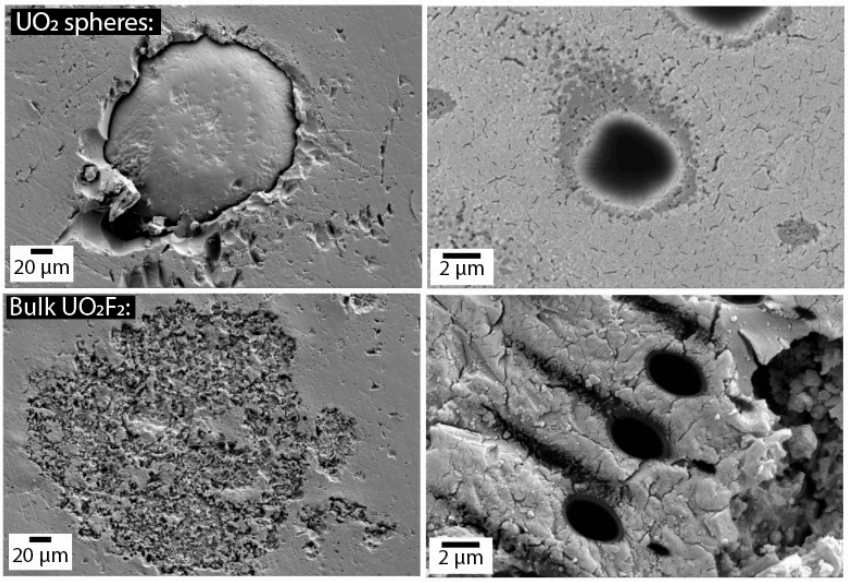

Figure 1. SEM images of two of the uranium compounds (UO_2 and UO_2F_2) on the epoxy mount, showing representative 200 pA analytical craters. (Note, craters were made before the analyses conducted in this study, and the mount containing these materials was further polished before NanoSIMS analysis).

2.3. NanoSIMS Analysis and Data Processing

The isotopic measurements reported in this study were performed using a NanoSIMS 50 L at Oak Ridge National Laboratory in November 2018. An additional session focused solely on UO_2 mounted on different substrates was conducted in March of 2019. The NanoSIMS platform, including important differences relative to other SIMS instruments, is described in [12]. An important note is that the instrument used in this study is equipped with the new Hyperion-II radio frequency plasma oxygen ion source (described in [24,25]), which was used to generate the O^- beam used in this study. For isotopic measurements, the NanoSIMS primary column was tuned to achieve a ~200 pA beam of O^- with a diameter of ~1 µm at the sample surface (Figure 1). This tuning was achieved primarily through the use of the L1 and L0 lenses in addition in combination with the D1 aperture. This beam was used for all analyses and tuning during the November 2018 session, with analyses performed using a static primary beam on the surface of the sample. The only exception to the beam current condition were analyses performed on the UO_2 sphere, which were made using progressively lower beam currents (200 pA, 150 pA, 100 pA, 50 pA, and 20 pA). These lower beam currents were achieved by lowering the value on the L1 lens.

While the instrument was operated at an MRP of ~7000 (defined as M/ΔM and achieved through the use of entrance and aperture slits as well as adjustments to the quadrupole lens), the physical properties of the NanoSIMS magnet means that it is impossible to collect ^{235}U and ^{238}U in the same magnetic field. It is also impossible to collect the $^{235}U^{16}O$ and $^{238}U^{16}O$ in the same magnetic field. Therefore, magnetic peak hopping was used. During each analysis, the magnet was stepped through four fields. The first field was used for settling the magnet, the second field contained ^{235}U, the third field contained $^{235}U^{16}O$, and the fourth field contained ^{238}U, $^{238}U^{16}O$, and $^{238}U^{16}O_2$. Please note that ^{235}U and ^{238}U, as well as $^{235}U^{16}O$ and $^{238}U^{16}O$, were measured on the same detectors in the different magnetic fields. Each analysis consisted of 20 cycles through the four magnetic fields, with a 10 s/cycle count time on each mass of interest. These conditions were used for all the materials. Between materials, minor tuning of the secondary ion extraction lens and secondary ion beam steering plates was done to compensate for differences in the sample height. An important note is that no formal presputtering routine was built into the analytical sequence. This was because the secondary ion signal was observed to achieve a maximum within a few seconds of the primary beam hitting the sample surface, so it was

decided that no presputtering was necessary for implantation purposes. Furthermore, there is a short period (<10 s) at the beginning of each analysis during which the primary beam dwells on the sample surface before the magnet begins cycling. As described below, the first two cycles of data collected during each analysis were excluded from consideration.

The raw data (counts observed at each cycle of data) was exported into Microsoft® Excel for processing. To generate $^{235}U/^{238}U$ and $^{235}U^{16}O/^{238}U^{16}O$ ratios for each analysis, the counts of ^{235}U and $^{235}U^{16}O$ observed during each cycle of data (lasting 10 s) were linearly extrapolated to the timestamp of ^{238}U, $^{238}U^{16}O$, and $^{238}U^{16}O_2$ (which were all collected in the same magnetic field). This was necessary as the secondary ion intensity was observed to change during each analysis (lasting approximately 45 min). In contrast, the 44 ns deadtime was found to be inconsequential because of the relatively low count rates obtained in this study (typically <10,000 cps), so a deadtime correction was not applied. Using this approach, a $^{235}U/^{238}U$ and $^{235}U^{16}O/^{238}U^{16}O$ ratios were generated for each cycle of the 20 cycles of data during a single analysis. The cycle-by-cycle values for the final 18 cycles of data collected during each analysis were then averaged together, with the standard deviation associated with this average used as the 1 standard deviation (1σ) uncertainty for each analysis.

For the UO_2 that was prepared specifically to assess questions over the role of sample preparation on the $^{235}U/^{238}U$ vs. $^{235}U^{16}O/^{238}U^{16}O$ ratios that arose during data interpretation, an additional session on the NanoSIMS was conducted in March of 2019. In this session, analytical conditions were nearly identical (e.g., same mass table/detector configuration, same analysis duration, same data processing approach) to those described above, except that a 100 pA primary beam was scanned over a 5 × 5 μm area for each analysis (as opposed to being used in static mode). Using this approach, data was collected for the UO_2 mounted in epoxy and dispersed onto the sticky carbon tab, but an operational issue prevented us from carrying out a full set of measurements on the UO_2 pressed into Indium. Additionally, a series of scans using the Cameca® Bar Graph software from mass 248 to 258 were conducted on the UO2 in epoxy, on the sticky carbon tab, and pressed into Indium using the 100 pA primary beam scanned over a 5 × 5 μm area.

2.4. Solution MC-ICP-MS

Following NanoSIMS analysis, stainless steel tweezers were used to excavate a portion of each uranium compound, and then transfer the excavated material into 0.5 mL of 4 M HNO_3. After 72 h of digestion at ambient conditions, the major uranium ratio for these solutions were determined on a Thermo Scientific NeptunePlus MC-ICP-MS. The instrument was equipped with the nuclear package and a jet interface. During analysis ^{235}U was placed on the L5 Faraday cup connected to a 10^{13} Ω amplifier, and ^{238}U was located on L4 Faraday cup connected to a 10^{11} Ω amplifier. The amplifiers were calibrated electronically with a 0.3 gain calibration card. The tau factor as well as a 20-min Faraday cup baseline measurement were performed. Sample solutions were introduced with a ~52 μL min^{-1} Elemental Scientific Inc. integrated PFA nebulizer into a quartz Elemental Scientific Inc. Apex Omega. The instrument sensitivity was ~1.4 V of signal per nanogram of uranium. The unknown samples were analyzed using standard sample bracketing method with 2% HNO_3 washout blanks placed before each standard/sample. Mass fraction corrections were determined with New Brunswick Laboratory Program Office Certified Reference Material U010. Unknown solutions were corrected for mass fractionation, instrument blank, baseline, and gain using established protocols in the Nuclear Analytical Chemistry and Isotopics Laboratory at Oak Ridge National Laboratory. Controls of IRMM 183, IRMM 184, and Oak Ridge National Laboratory WRM were analyzed throughout the sequence to monitor instrument operation. Final calculated isotopic values were provided with Guide to Uncertainty in Measurement-compliant uncertainties.

3. Results

The ratios reported in Table S1, which were determined using NanoSIMS as described in Section 2.3, are uncorrected for mass fractionation. Additionally, the 1σ uncertainties associated with these ratios

are simply the standard deviation associated with the final 18 cycles of data collected during each analysis. While it is common to apply a standard reference material-based mass fractionation correction, as well as to factor the variability of standards measurement into the determination of uncertainty for unknowns, when reporting isotope data, applying correction factors, and combining uncertainties would complicate the aims of this study, which are to understand the effects of different analytical approaches on the raw data.

In Figure 2, the percent uncertainty, calculated as 1σ associated with the average of the ratios observed for each cycle of data for each analysis, on the $^{235}U/^{238}U$ (Figure 2a) and $^{235}U^{16}O/^{238}U^{16}O$ ratios (Figure 2b) as a function of the total number of counts of ^{235}U (Figure 2a) and $^{235}U^{16}O$ (Figure 2b) observed during each analysis of the UO_2 sphere's polished cross section. As described in Section 2, a variety of beam currents were used to analyze the UO_2, resulting in a wide spread in total observed counts for this material. In contrast, the other materials were only analyzed using the 200 pA beam current, resulting in a much narrower spread in count rate. Therefore, the type of plot shown in Figure 2 is only representative of the UO_2 sphere. In Figure 3, each analysis of $^{235}U/^{238}U$ (Figure 3a) and $^{235}U^{16}O/^{238}U^{16}O$ (Figure 3b) and its associated 1σ internal precision for the UO_2 sphere is shown relative to the solution MC-ICP-MS value for the UO_2. Individual analyses are grouped according to the five primary beam currents (200 pA, 150 pA, 100 pA, 50 pA, and 20 pA) that were used to analyze the UO_2 sphere. In Figure 4 each analysis's deviance in the $^{235}U/^{238}U$ (Figure 4a) and $^{235}U^{16}O/^{238}U^{16}O$ (Figure 4b) ratios relative to the solution MC-ICP-MS value is plotted as a function of the total number of counts of ^{235}U (Figure 4a) and $^{235}U^{16}O$ (Figure 4b) observed during each analysis for the UO_2 sphere.

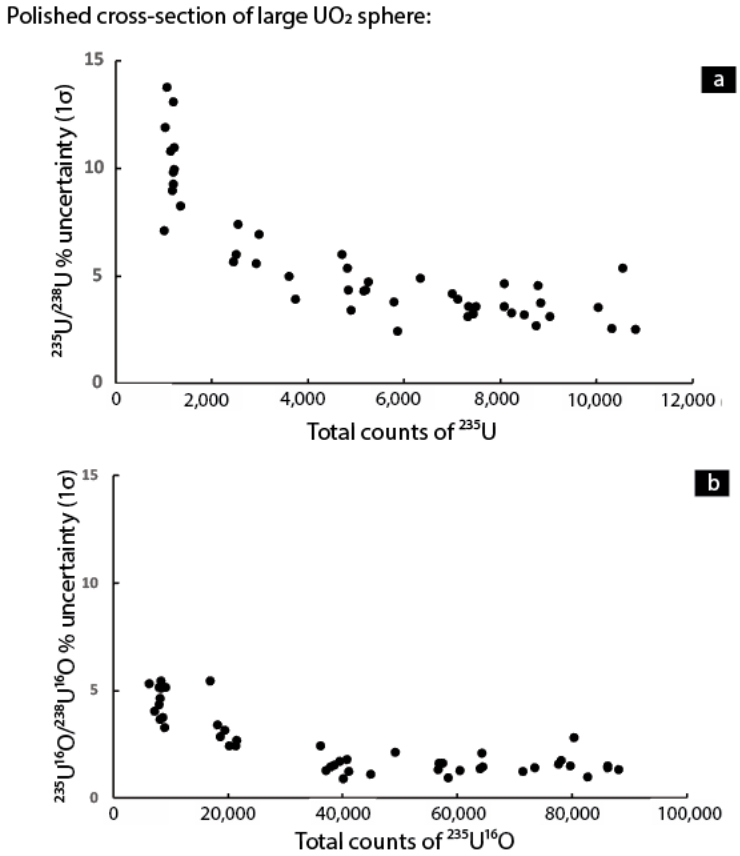

Figure 2. Plot of the percent uncertainty, calculated as 1σ associated with the average of the ratios observed at each cycle of data during each analysis, on the (**a**) $^{235}U/^{238}U$ and (**b**) $^{235}U^{16}O/^{238}U^{16}O$ ratios as a function of the total number of counts of (**a**) ^{235}U and (**b**) $^{235}U^{16}O$ observed during each analysis of the UO_2 sphere's polished cross section.

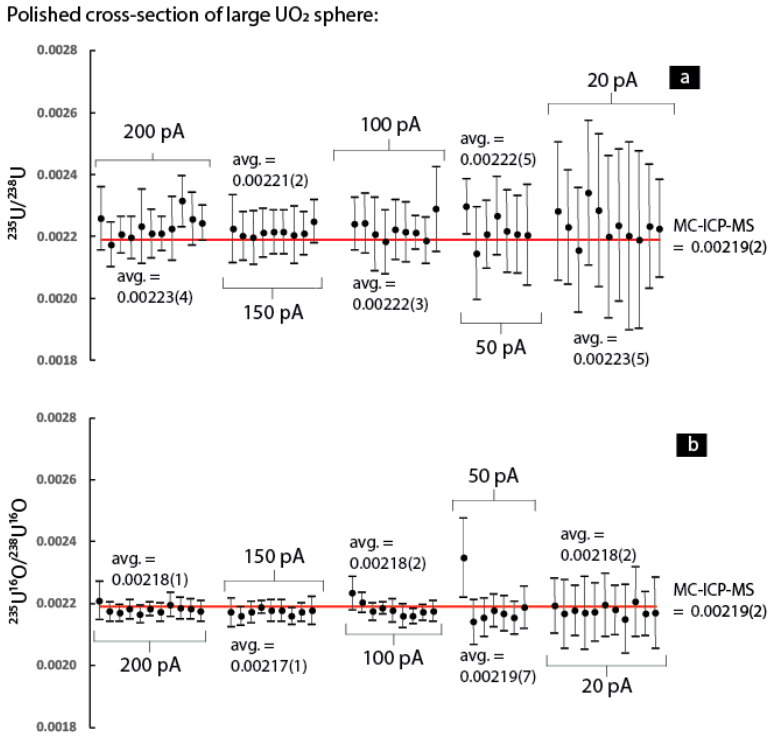

Figure 3. Plot of each analysis's (**a**) $^{235}U/^{238}U$ and (**b**) $^{235}U^{16}O/^{238}U^{16}O$ ratio and its associated 1σ uncertainty for the UO_2 sphere is shown relative to the solution MC-ICP-MS value (red line). Individual analyses are grouped according to the five primary beam currents (200 pA, 150 pA, 100 pA, 50 pA, and 20 pA) that were used to analyze the UO_2 sphere.

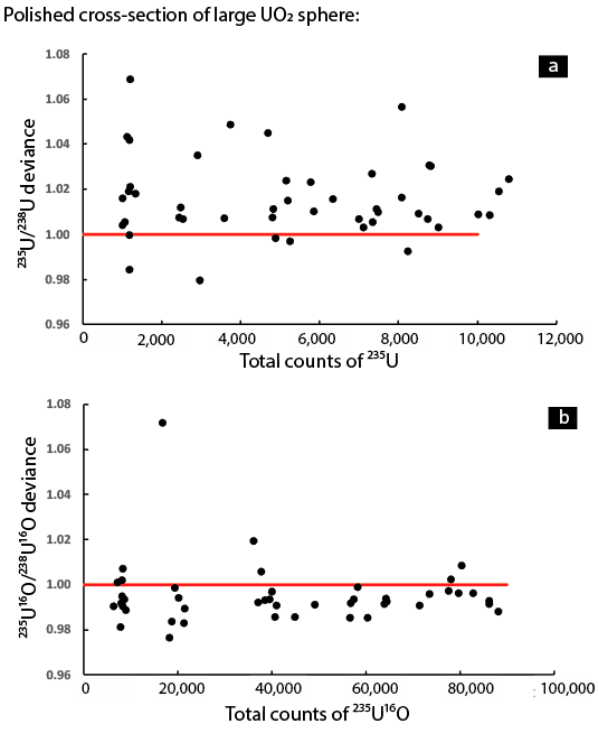

Figure 4. For the UO_2 sphere, each analysis's deviance in the (**a**) $^{235}U/^{238}U$ and (**b**) $^{235}U^{16}O/^{238}U^{16}O$ ratio relative to the solution MC-ICP-MS value (red line) is plotted as a function of the total number of counts of (**a**) ^{235}U and (**b**) $^{235}U^{16}O$ observed during each analysis.

In Figures 5 and 6, each analysis of $^{235}U/^{238}U$ and $^{235}U^{16}O/^{238}U^{16}O$ and its associated 1σ uncertainty is shown relative to the solution MC-ICP-MS values for the UO_2F_2 (Figure 5a,b) and UO_3 (Figure 6a,b). In Figures 7 and 8, each analysis of $^{235}U/^{238}U$ and $^{235}U^{16}O/^{238}U^{16}O$ and its associated 1σ uncertainty for the UF_4 (Figure 7a,b) and $UO_2(NO_3)_2{\cdot}6(H_2O)_3$ (Figure 8a,b) is shown. In Figure 9, each analysis of $^{235}U/^{238}U$ and $^{235}U^{16}O/^{238}U^{16}O$ and its associated 1σ uncertainty for the NIST-610 glass (Figure 9a,b) is shown relative to the reference $^{235}U/^{238}U$ of 0.00239, which is the average LG-SIMS value reported in [21]. In Figure 10, each analysis's $^{235}U/^{238}U$ and $^{235}U^{16}O/^{238}U^{16}O$ and its associated 1σ uncertainty for Plesovice zircon reference material (Figure 10a,b) is analyzed using the 200 pA primary beam current is shown relative to the natural $^{235}U/^{238}U$ of 0.00726, which is the consensus value reported in [23]. For both materials, the uncertainties reported in the literature are far below the internal precision level achieved via the NanoSIMS.

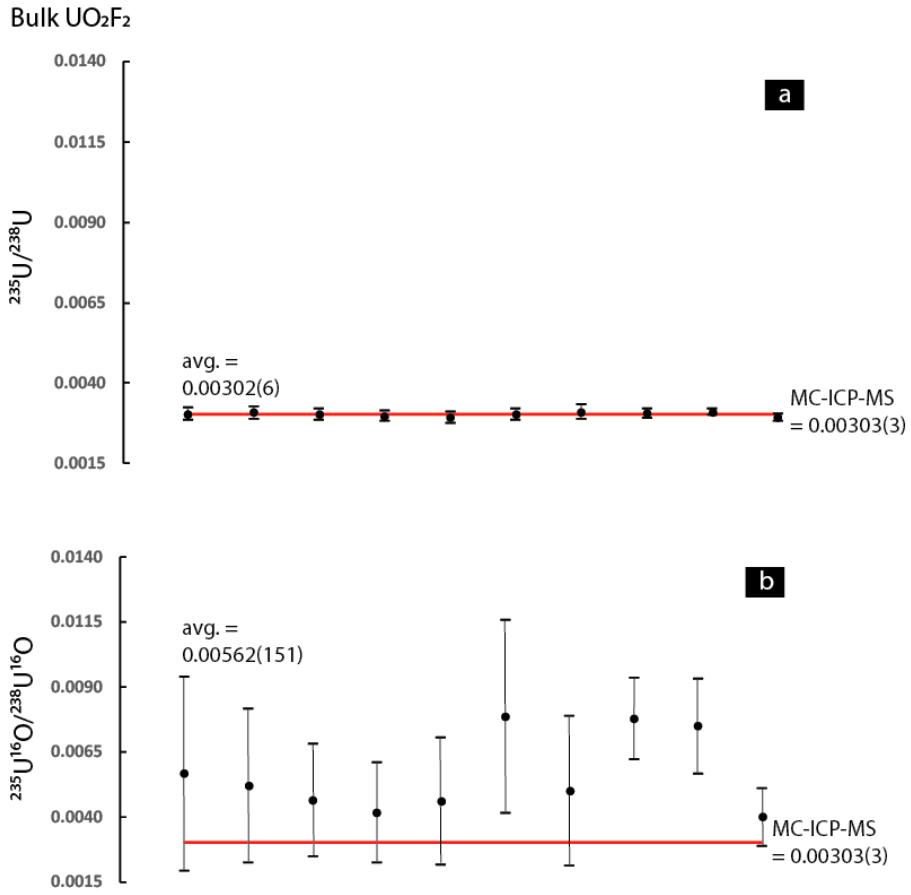

Figure 5. Plot of each analysis's (**a**) $^{235}U/^{238}U$ and (**b**) $^{235}U^{16}O/^{238}U^{16}O$ ratio and its associated 1σ uncertainty relative to the solution MC-ICP-MS values (red line) for the UO_2F_2.

For the UO_2 sphere, the average NanoSIMS $^{235}U/^{238}U$ ratio and its associated 1σ uncertainty for the 200 pA, 150 pA, 100 pA, 50 pA, and 20 pA primary beam currents were 0.00223 ± 0.00004, 0.00221 ± 0.00002, 0.00222 ± 0.00003, 0.00222 ± 0.00005, and 0.00223 ± 0.0005, respectively. These values compare well with the solution value of 0.00219 ± 0.00002. For the various beam currents, the average of the 1σ uncertainties associated with the individual measurements made using each beam current are 0.00008 for the 200 pA and 150 pA settings. The 100 pA, 50 pA, and 20 pA settings produced slightly higher average uncertainties of 0.00010, 0.00013, and 0.00023, respectively. For the $^{235}U^{16}O/^{238}U^{16}O$ ratio, average ratios and associated 1σ uncertainties, for the 200 pA, 150 pA, 100 pA, 50 pA, and 20 pA primary beam currents were 0.00218 ± 0.00001, 0.00217 ± 0.00001, 0.00218 ± 0.00001, 0.00219 ± 0.00007, and 0.00218 ± 0.0002, respectively. These values align more closely with the solution value 0.00219 ± 0.00002 instead of the $^{235}U/^{238}U$ ratios. For the various beam currents, the average of

the 1σ uncertainties associated with the individual measurements made using each beam current are 0.00003 for the 200 pA, 150 pA, and 100 pA settings. The 50 pA and 20 pA settings produced slightly higher average uncertainties of 0.00007 and 0.00010, respectively.

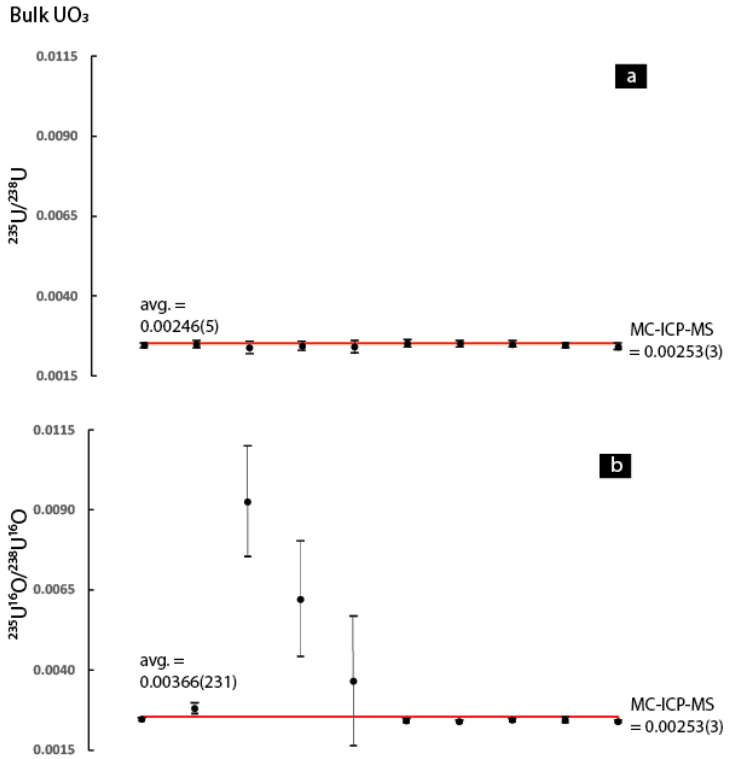

Figure 6. Plot of each analysis's (**a**) $^{235}U/^{238}U$ and (**b**) $^{235}U^{16}O/^{238}U^{16}O$ ratio and its associated 1σ uncertainty relative to the solution MC-ICP-MS value (red line) for the and UO_3 analyzed using the 200 pA primary beam current.

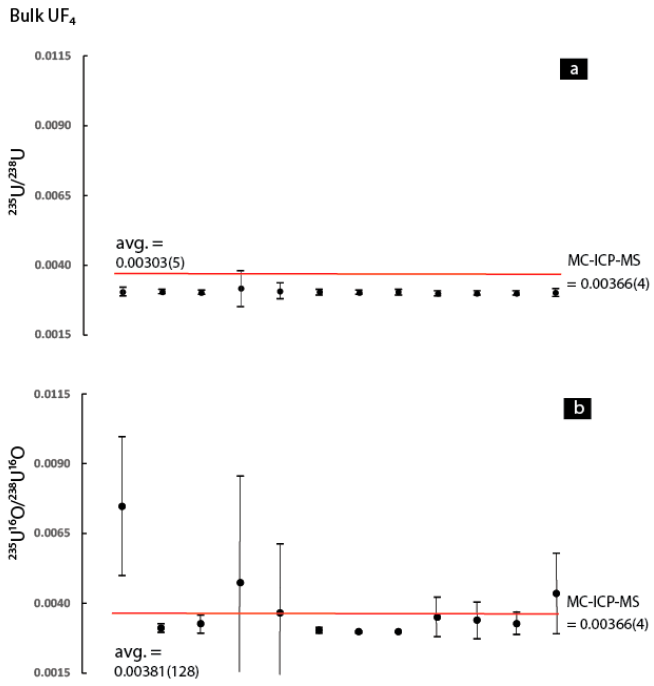

Figure 7. Plot of each analysis's (**a**) $^{235}U/^{238}U$ and (**b**) $^{235}U^{16}O/^{238}U^{16}O$ ratio and its associated 1σ uncertainty, relative to the solution MC-ICP-MS value (red line), for the UF_4.

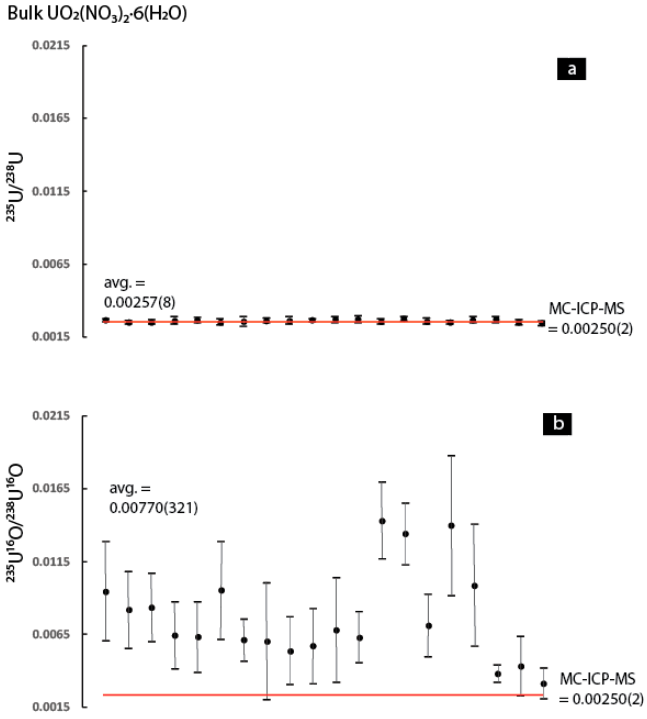

Figure 8. Plot of each analysis's (**a**) $^{235}U/^{238}U$ and (**b**) $^{235}U^{16}O/^{238}U^{16}O$ ratio and its associated 1σ uncertainty relative to the solution MC-ICP-MS value (red line), for $UO_2(NO_3)_2{\cdot}6(H_2O)$ analyzed using the 200 pA primary beam.

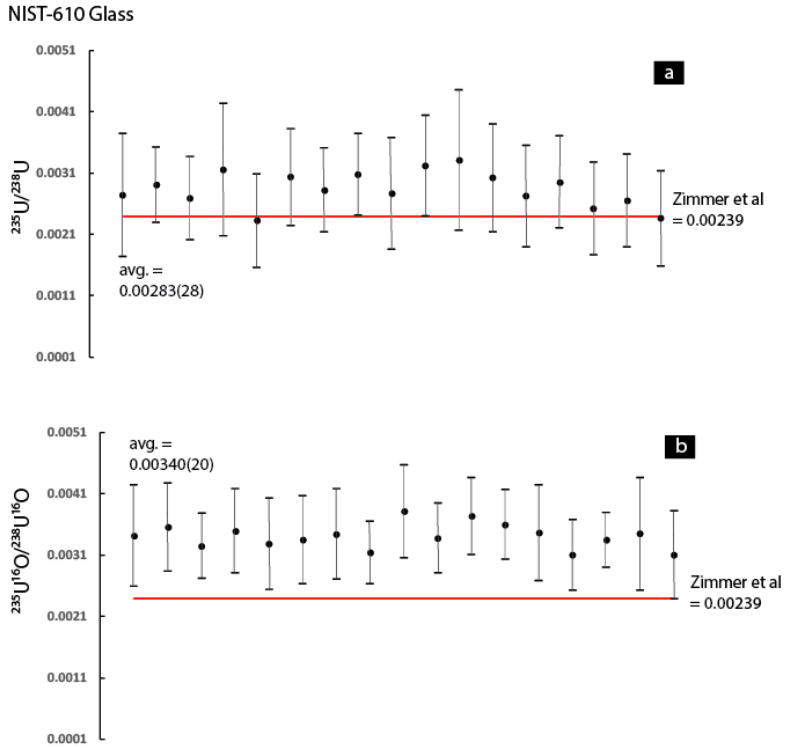

Figure 9. Plot of each analysis's (**a**) $^{235}U/^{238}U$ and (**b**) $^{235}U^{16}O/^{238}U^{16}O$ ratio and its associated 1σ uncertainty, for the NIST-610 glass. The reference $^{235}U/^{238}U$ ratios (red line) for the NIST-610 glass is the average LG-SIMS value reported in [22]. Uncertainty of the value in [22] is considerably lower than the NanoSIMS results and is therefore not shown here.

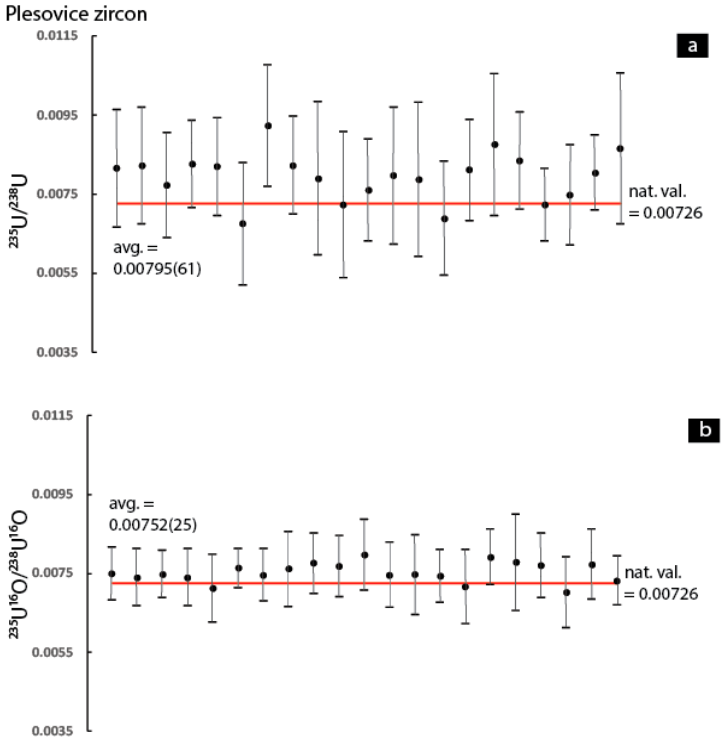

Figure 10. Plot of each analysis's (**a**) $^{235}U/^{238}U$ and (**b**) $^{235}U^{16}O/^{238}U^{16}O$ ratio and its associated 1σ uncertainty, for Plesovice zircon reference material analyzed using the 200 pA primary beam current and shown relative to the natural $^{235}U/^{238}U$ of 0.00726 (red line) reported in [23]. Uncertainty of the value in [23] is considerably lower than the NanoSIMS results and is therefore not shown here.

While solution data was not obtained for the NIST-610 glass and Plesovice zircon reference materials analyzed in this study, there is an LG-SIMS $^{235}U/^{238}U$ ratio available for the NIST-610 glass published in [21], whereas the Plesovice zircon (described in [22]) can be assumed to have a natural $^{235}U/^{238}U$ ratio. For the NIST-610 glass, which was only analyzed using the 200 pA beam current, the average $^{235}U/^{238}U$ and $^{235}U^{16}O/^{238}U^{16}O$ ratios and associated 1σ uncertainties were 0.00283 ± 0.00028 and 0.00340 ± 0.00020. Considering uranium occurs at the parts per million level in the NIST-610 glass and that only a 200 pA primary beam current was used, both values compare well with the published $^{235}U/^{238}U$ ratio of 0.00239 [21] (note the uncertainty of the published ratio is in the seventh decimal place). For the NIST-610 glass, the average 1σ uncertainty of the individual $^{235}U/^{238}U$ ratios is slightly higher at 0.00084 compared to the $^{235}U^{16}O/^{238}U^{16}O$ ratios at 0.00067. For the Plesovice zircon, which was only analyzed using the 200 pA beam current and is assumed to have a natural $^{235}U/^{238}U$ ratio of 0.00726 [23], the average $^{235}U/^{238}U$ and $^{235}U^{16}O/^{238}U^{16}O$ ratios and associated 1σ uncertainties were 0.00795 ± 0.00061 and 0.00752 ± 0.00025. Like the NIST-610 glass, the average 1σ uncertainty of the individual $^{235}U/^{238}U$ ratios of the Plesovice zircon is slightly higher at 0.00146 compared to the $^{235}U^{16}O/^{238}U^{16}O$ ratios at 0.00080.

As described in Sections 2.2 and 2.3, an additional NanoSIMS session was conducted in March 2019 to assess the role of sample preparation on the $^{235}U/^{238}U$ vs. $^{235}U^{16}O/^{238}U^{16}O$ ratios. Data from the UO_2 prepared specifically for this session can be found in its own section at the end of Table S1, and was not included in the UO_2 results described above. The mass scans described in Section 2.3 can be found in Table S2. In Figure 11, it is possible to compare the $^{235}U/^{238}U$ vs. $^{235}U^{16}O/^{238}U^{16}O$ for the UO_2 dispersed onto the sticky carbon tab (Figure 11a) versus the UO_2 mounted in epoxy (Figure 11b); As noted in Section 2.3, a full dataset was not acquired for the UO_2 pressed into Indium. In Figure 11, the $^{235}U/^{238}U$ ratios, and their complimentary (e.g., from the same analysis) $^{235}U^{16}O/^{238}U^{16}O$ ratios, are grouped together and provided side-by-side in identical order (as opposed to the vertically stacked format used in Figures 3 and 5, Figures 6–10). Mass scans ranging from mass 248 to 258 are provided

as insets on Figure 11 (a full dataset from these mass scans can be found in Table S2, in addition to the mass scan data from the UO_2 pressed into Indium), and it is noteworthy (see discussion Section 4.3) that the $^{238}U^{12}C$ peak at mass ~250 is visible in the mass scans conducted on the UO_2 dispersed onto the sticky carbon tab as well as mounted in epoxy. For the UO_2 analyzed during this additional session, both the $^{235}U/^{238}U$ and $^{235}U^{16}O/^{238}U^{16}O$ ratios (refer to Table S1) compare well with the solution ICP-MS $^{235}U/^{238}U$ value of 0.00219 ± 0.00002 determined from UO_2 taken from the same batch of material.

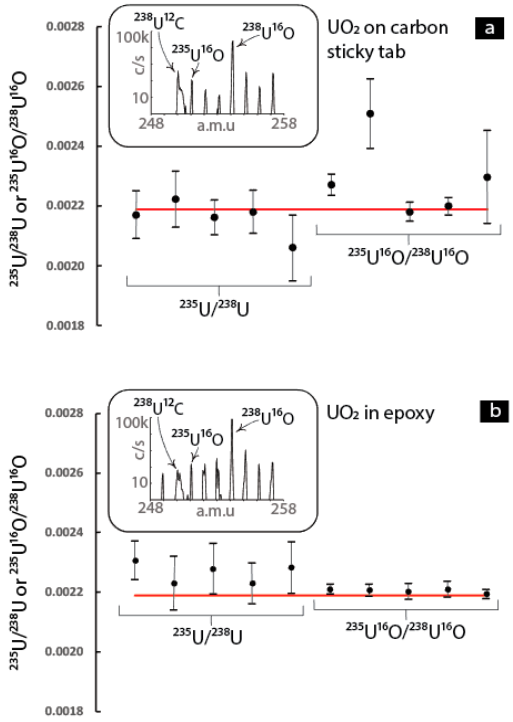

Figure 11. Comparison of $^{235}U/^{238}U$ vs. $^{235}U^{16}O/^{238}U^{16}O$ for UO_2 that was mounted in epoxy (**a**) as well as dispersed on a sticky carbon tab (**b**). Mass scans, from mass 248 to 258, acquired for both sample preparation approaches are shown as insets. While the $^{238}U^{12}C$ peak is visible in both scans, the $^{238}U^{12}C$ peak is ~1000 counts/second for the UO_2 dispersed on the sticky carbon tab whereas it is ~100 counts/second for the UO_2 mounted in epoxy. The $^{235}U/^{238}U$ and $^{235}U^{16}O/^{238}U^{16}O$ data used to construct these plots were collected in a separate session (March 2019) and can be found in their own section at the end of Table S1, while the mass scan data can be found in Table S2.

4. Discussion

4.1. Previous Investigations into the Controls on Secondary ion Yields during SIMS Analysis

In the broader SIMS community, there are many questions about the sputtering and ionization processes (see discussion by [13]). Although models that produce testable predictions based on the relative yields between secondary monatomic and molecular secondary ion species have been developed (e.g., the local thermodynamic equilibrium model of [26]), the reality is that the secondary ion yields are dependent on so many factors (e.g., composition of the target, the particular element in question, the nature of the primary beam, the secondary ion extraction geometry of the instrument itself, etc.) that it has proven difficult to develop a unified sputtering and ionization model that fully explains secondary ion yield observations. Uncertainty in the debate over what actually controls ionization [27–31] is compounded by the fact that only a small fraction of the sputtered material, which is a mixture of both monatomic, molecular, and polyatomic species, acquires a charge such that it can be extracted and transmitted through the SIMS instrument's ion optical system. Similarly, ions that are part of the primary beam itself are implanted into material being sputtered, further complicating the

development of a unified theory of ionization. While there are still uncertainties about the sputtering and ionization processes, a basic observation of SIMS data is that there are sometimes relatively fixed relationships between the secondary ion production rates of monatomic elemental species and their respective molecular elemental oxide secondary ions.

For example, [32] found that when $ZrSiO_4$ is sputtered with 10,000 V O^-, $YbO^+/Yb^+ \approx 0.5$, whereas $HfO^+/Hf^+ \approx 4.0$ and $YbO_2{}^+/YbO^+ < 0.001$. In contrast, a brief survey of the U-Pb SIMS literature indicates that the measured secondary ion signals for $ZrSiO_4$ are $^{238}U^{16}O > {}^{238}U^{16}O_2 > {}^{238}U$ (see discussion by [33]). The relatively consistent relationship between the observed ^{238}U, $^{238}U^{16}O$, and $^{238}U^{16}O_2$ secondary ions produced when $ZrSiO_4$ is sputtered with an O^- or $O_2{}^-$ primary beam form the cornerstone of U-Pb dating by SIMS (see discussions by [15,33,34]) because an interelement correction factor, which is necessary to obtain accurate $^{206}Pb/^{238}U$ ratios, can be derived from the relationships between the ^{238}U, $^{238}U^{16}O$, and $^{238}U^{16}O_2$ secondary ion species. Although it is generally accepted that the element and elemental oxide secondary ion relationships can behave consistently within a given type of matrix, there have not been any systematic attempts to use this behavior as means of improving the precision of the $^{235}U/^{238}U$ ratio determination by looking at $^{235}U^{16}O$ and $^{238}U^{16}O$, which can have higher count rates than the ^{235}U and ^{238}U elemental secondary ions (see discussion by [3]). Instead, considerable energy has been devoted to understanding oxide formation rates for correcting isobaric interferences and monitoring energy filtering regimes.

4.2. Does Use of the $^{235}U^{16}O/^{238}U^{16}O$ Improve Precision and Accuracy at Low Count Rates?

For any isotope ratio determination, the total uncertainty is a combination of uncertainty associated with the count rate, the behavior of standards, the robustness of the mass fractionation correction regime, inter-detector calibration issues, as well as other factors. For SIMS, as with all mass spectrometric isotope ratio determinations, there are a variety of approaches to constraining and combining these uncertainties (see discussion by [4]). However, it is indisputable that two major contributors to the precision and accuracy of any SIMS measurement are (1) the stability of the isotope ratio, as reflected by the standard deviation, during each analysis, and (2) the deviance of the raw (e.g., uncorrected) ratio relative to the 'true' value for the matrix in question. For the $^{235}U/^{238}U$ ratio, both are known to vary proportionally with the count rate of ^{235}U (when ^{235}U is the minor isotope). For all the materials examined in this study, the secondary ion count rates of $^{235}U^{16}O$ and $^{238}U^{16}O$ were considerably higher than the ^{235}U and ^{238}U (exceptions are discussed in Section 4.3).

As described in Section 2, the UO_2 was analyzed using a variety of primary beam currents ranging from 200 pA down to 20 pA. This resulted in a wide range of total counts for ^{235}U and $^{235}U^{16}O$ that enable a robust assessment of the effect of using the $^{235}U^{16}O/^{238}U^{16}O$ compared to the $^{235}U/^{238}U$ ratio. In Figure 2, which is a plot of the percent uncertainty, calculated as 1σ associated with the average of the ratios observed at each cycle of data during each analysis, on the $^{235}U/^{238}U$ (Figure 2a) and $^{235}U^{16}O/^{238}U^{16}O$ ratios (Figure 2b) as a function of the total number of counts of ^{235}U (Figure 2a) and $^{235}U^{16}O$ (Figure 2b) observed during each analysis of the UO_2 sphere's polished cross section, there is a clear improvement in the standard deviation associated with each individual measurement when the $^{235}U^{16}O/^{238}U^{16}O$ ratio is used. This is also evident in Figure 3, which plots each analysis's $^{235}U/^{238}U$ (Figure 3a) and $^{235}U^{16}O/^{238}U^{16}O$ ratios (Figure 3b) and its associated 1σ uncertainty for the UO_2 sphere. In Figure 3, the individual analyses are grouped according to the five primary beam currents (200 pA, 150 pA, 100 pA, 50 pA, and 20 pA) that were used to analyze the UO_2 sphere and are also shown relative to the solution MC-ICP-MS value. Clearly, there is a reduction in the standard deviation associated with each measurement. In Figure 3, it is also evident that the raw isotope ratios fall closer to the solution MC-ICP-MS value when the $^{235}U^{16}O/^{238}U^{16}O$ ratio is used. This observation is further bolstered by Figure 4, where each analysis's deviance in the $^{235}U/^{238}U$ (Figure 4a) and $^{235}U^{16}O/^{238}U^{16}O$ (Figure 4b) ratios relative to the solution MC-ICP-MS value are plotted as a function of the total number of counts of ^{235}U (Figure 4a) and $^{235}U^{16}O$ (Figure 4b) observed during each analysis.

For the UO_2 analyzed in this study, use of the $^{235}U^{16}O/^{238}U^{16}O$ ratio appears to result in improved accuracy and precision. However, because the atomic-to-molecular secondary ion formation rate and general behavior is matrix dependent, it is necessary to consider whether this behavior is present in the other matrices examined in this study. While the UO_2 was the only material that was investigated using multiple primary beam currents, the comparison of the $^{235}U/^{238}U$ versus the $^{235}U^{16}O/^{238}U^{16}O$ acquired using only a 200 pA beam current should still provide a preliminary indication of whether the observations made on UO_2 can be extended to the other uranium compounds. In Figures 5–8, which are plots of each measured $^{235}U/^{238}U$ and $^{235}U^{16}O/^{238}U^{16}O$ ratio, and their associated 1σ uncertainty for the UO_2F_2 (Figure 5a,b), UO_3 (Figure 6a,b), $UO_2(NO_3)_2{\cdot}6(H_2O)$ (Figure 7a,b), and UF_4 (Figure 8a,b), it is clear that the observations made on UO_2 cannot be extended uniformly to the other uranium compounds. This is because for many of the analyses, there is considerably higher standard deviation when the $^{235}U^{16}O/^{238}U^{16}O$ ratio is used. Additionally, when the NanoSIMS data is compared with the MC-ICP-MS $^{235}U/^{238}U$ ratios (UO_2F_2 in Figure 5, and UO_3 in Figure 6, $UO_2(NO_3)_2{\cdot}6(H_2O)$ in Figure 7, and UF_4 in Figure 8), it is clear that there is considerably more scatter relative to the solution value when the $^{235}U^{16}O/^{238}U^{16}O$ ratios are used for all of the uranium compounds except the UO_2. The scatter also appears decoupled from the $^{235}U/^{238}U$ ratios (e.g., for some analyses, the $^{235}U^{16}O/^{238}U^{16}O$ ratio deviates strongly from the solution value, but the $^{235}U/^{238}U$ ratio remains stable).

Therefore, it appears that use of the $^{235}U^{16}O/^{238}U^{16}O$ ratio would result in improved precision and accuracy for certain bulk chemistries (e.g., UO_2), but not others (e.g., UO_2F_2, UO_3, $UO_2(NO_3)_2{\cdot}6(H_2O)$, and UF_4). The reasons for this behavior will be discussed in the following section, but at this point it is also worth considering the behavior of matrices containing only trace levels of uranium. In Figures 9 and 10, each analyses of $^{235}U/^{238}U$ and $^{235}U^{16}O/^{238}U^{16}O$ ratio, and their associated 1σ uncertainties, for the NIST-610 glass (Figure 9a,b) and Plesovice zircon (Figure 10a,b) are shown relative to the reference values (refer to figure captions) for these materials. For the NIST-610 glass, there is a slight improvement in the uncertainty of the individual measurements when the $^{235}U^{16}O/^{238}U^{16}O$ ratio is used, but this is accompanied by a slight shift further away from the 'true' $^{235}U/^{238}U$ ratio reported in [22]. In contrast, the data from the Plesovice zircon indicates a marked improvement in the uncertainty associated with the individual measurements as well as a decrease in the degree of deviance relative the natural $^{235}U/^{238}U$ ratio used as the 'true' value. The observation that the $^{235}U^{16}O/^{238}U^{16}O$ ratios have marked improvement for these two materials is an important observation considering that uranium is only present at a trace phase within these two matrices (ppm levels)—this is also evident by the considerably lower count rates for the atomic and molecular uranium secondary ion species relative to the uranium compounds (Table S1).

In summary, the data indicates that use of the $^{235}U^{16}O/^{238}U^{16}O$ ratio results in higher precision and better accuracy for the UO_2 as well as the two silicate reference materials. In contrast, for the UO_2F_2, UO_3, $UO_2(NO_3)_2{\cdot}6(H_2O)$, and UF_4 it is clear that the $^{235}U^{16}O/^{238}U^{16}O$ ratio is associated with considerably higher scatter (both within and between individual analyses) compared to the $^{235}U/^{238}U$. The implications of this observation for SIMS isotope ratio measurements will be discussed in the final section of the discussion. Now, the discussion will shift to a discussion of the possible mechanisms responsible for producing the sporadic results regarding improvement in the accuracy and precision when the $^{235}U^{16}O/^{238}U^{16}O$ ratio is used.

4.3. Possible Origins of the Inconsistent Behavior Between the $^{235}U/^{238}U$ and $^{235}U^{16}O/^{238}U^{16}O$ Across the Various Compounds

As described in the preceding section, an observation from the dataset is that use of the $^{235}U^{16}O/^{238}U^{16}O$ compared to the $^{235}U/^{238}U$ ratio results in improved accuracy and internal precision for the UO_2 and two silicate reference materials. In contrast, the accuracy and precision are considerably worse for the UO_2F_2, UO_3, $UO_2(NO_3)_2{\cdot}6(H_2O)$, and UF_4 when the $^{235}U^{16}O/^{238}U^{16}O$ is used. Three possible origins for this behavior will be explored in this discussion: (a) the SIMS 'matrix effect', (b) fluorine- and carbon-based interferences, and c) the effect of sample topography.

If only data from the uranium compounds were available, it would be reasonable to attribute the decrease in precision and accuracy to some type of matrix effect related to the presence of fluorine and nitrogen in the bulk matrices of the UO_2F_2, $UO_2(NO_3)_2{\cdot}6(H_2O)$, UO_3, and UF_4. The UO_3 examined in this study was prepared by calcination of $UO_2(NO_3)_2{\cdot}6(H_2O)$, but no additional steps were taken to remove residual nitrogen. Therefore, there is presumably residual nitrogen present in the UO_3 that was examined in this study. In such a scenario, it would be possible that nitrogen and fluorine contributed to scavenging of the oxygen ions available at the sputtering site, thus destabilizing the formation rate of the UO molecular ion. However, oxygen scavenging at the sputtering site does not explain why the results from the two silicate reference materials mirrored those from the UO_2 in that the $^{235}U^{16}O/^{238}U^{16}O$ resulted in improved accuracy and precision relative to the $^{235}U/^{238}U$ ratio. In considering that uranium is only present as a trace phase within these two silicate reference materials, there would have been an abundance of reactive ions available at the sputtering site to scavenge oxygen ions.

For the two fluorine bearing uranium compounds, it is also possible that $^{19}F^+$ combined with $^{235}U^+$ to form the $^{235}U^{19}F^+$ molecular secondary ion (mass = 254.0423262) that would require an MRP of (defined as M/ΔM) of 75,353, well above what as used in this study, to be separated from the $^{238}U^{16}O^+$ (mass = 254.045697622) molecular ion measured in this study. It is possible to assess whether $^{235}U^{19}F$ contributed to the observed secondary ion signal of $^{238}U^{16}O^+$ by looking at the $^{235}U^{16}O/^{238}U^{16}O$ ratios for the UO_2F_2 and UF_4 in Figures 5b and 7b. The presence of $^{235}U^{19}F^+$ would be expected to enhance the secondary ion signal observed at $^{238}U^{16}O^+$, thus resulting in a lower $^{235}U^{16}O/^{238}U^{16}O$ ratio. For the UO_2F_2 (Figure 5b), the individual $^{235}U^{16}O/^{238}U^{16}O$ ratios are consistently biased above the solution ICP-MS and NanoSIMS $^{235}U/^{238}U$ ratios (Figure 5a), whereas for the UF_4 (Figure 7b), the $^{235}U^{16}O/^{238}U^{16}O$ ratios are highly scattered but do tend to agree with the NanoSIMS $^{235}U/^{238}U$ ratios (Figure 7a), which are also biased below the solution ICP-MS value. Therefore, there does not appear to be a systematic or significant contribution from the $^{235}U^{19}F^+$ on the $^{238}U^{16}O^+$ signal.

It is also necessary to consider the possibility that $^{238}U^{13}C^+$ (mass = 251.054138) and $^{238}U^{12}C^1H^+$ (mass = 251.058608) molecular ions interfered with the observed $^{235}U^{16}O^+$ secondary ion signal (mass = 251.038837622). Because MRP values of 16,408 and 12,698 would be needed to separate the potential $^{238}U^{13}C^+$ and $^{238}U^{12}C^1H^+$ interferences on $^{235}U^{16}O^+$, respectively, and the fact that carbon from the epoxy or polishing compound may have contaminated, and then become trapped, in the uranium compounds with irregular surfaces, it is fully possible that a portion of the $^{235}U^{16}O^+$ signal was derived from carbon-based molecular interferences. $^{238}U^{13}C^+$ and $^{238}U^{12}C^1H^+$ would be expected to increase the observed $^{235}U^{16}O^+$ secondary ion signal, thus biasing the $^{235}U^{16}O/^{238}U^{16}O$ ratio toward elevated values. Examination of the results from the UO_2F_2, $UO_2(NO_3)_2{\cdot}6(H_2O)$, UO_3, and UF_4 (Figures 5–7) reveals that some of the individual $^{235}U^{16}O/^{238}U^{16}O$ ratios display a marked positive bias, suggesting that carbon-based molecular interferences may have contributed to the instability of the $^{235}U^{16}O/^{238}U^{16}O$ ratios relative to the $^{235}U/^{238}U$ ratios from these samples. However, it is important to note that the $^{235}U^{19}F^+$ molecular interference on $^{238}U^{16}O$ would have an opposite effect to the carbon-based molecular interferences on the $^{235}U^{16}O/^{238}U^{16}O$ ratio, so understanding the interplay between these two potential interferences is not straightforward.

While the effects of fluorine- and carbon-based molecular interferences on the measured $^{235}U^{16}O/^{238}U^{16}O$ ratios cannot be ruled out, fully evaluating this potential mechanism as the cause of destabilization of the $^{235}U^{16}O/^{238}U^{16}O$ ratios is complicated by the fact that there are no data available to independently assess the rate at which these potential molecular interferences were formed. While it may theoretically be possible to monitor the intensity of the $^{238}U^{12}C$ molecular species, and then use this information to subtract the inferred $^{238}U^{13}C$ contribution to the $^{235}U^{16}O$ signal, this would require a different detector and magnetic field setup than what was used in this study, and therefore no such data are available. It would also be necessary to account for the $^{238}U^{12}C^1H$ hydride formation rate. To more fully understand the magnitude of the $^{238}U^{13}C$ contribution to the $^{235}U^{16}O$ signal,

an additional analytical session was conducted in March 2019 whereupon data collected from UO_2 dispersed onto a sticky carbon tab could be compared with data collected from UO_2 mounted in epoxy.

Examination of the insets on Figure 11 reveals that the $^{238}U^{12}C$ molecular species can be observed in both sample preparation approaches (the sticky carbon tab as well as the epoxy). Examination of a mass scan conducted on UO_2 pressed into Indium (provided in Table S2) reveals no signal at the $^{238}U^{12}C$ molecular species, suggesting that the source of carbon is indeed related to the sample preparation (e.g., contamination introduced during grinding/polishing) and sticky carbon Table For the UO_2 on the sticky carbon tab, the $^{238}U^{12}C$ molecular species achieves a maximum of ~400 c/s (Table S2), whereas for the UO_2 in epoxy, it achieves a maximum of ~65 c/s (Table S2). Using the natural abundance of ^{13}C (1.07%), the expected count rate for the $^{238}U^{13}C$ interference on $^{235}U^{16}O$ would be ~4.3 c/s for the UO_2 dispersed on the sticky carbon tab and ~0.7 c/s for the UO_2 in epoxy. For the UO_2 dispersed on the sticky carbon tab, this would account for ~3.7% of the signal at the $^{235}U^{16}O$ mass position. For the UO_2 mounted in epoxy, the contribution is ~0.5%.

Based on these considerations, it does appear that if a significant amount of carbon is present within the analytical volume (as would be expected for the UO_2 dispersed onto the sticky carbon tab), the $^{235}U^{16}O/^{238}U^{16}O$ ratio would be expected to exhibit a few % positive deviation relative to the $^{235}U/^{238}U$. In contrast, where only trace amounts of carbon are present (as would be expected for the UO_2 mounted in epoxy), the effect would be considerably less. This prediction is born out in Figure 11, where it can be seen that some of the $^{235}U^{16}O/^{238}U^{16}O$ values from the UO_2 dispersed onto the sticky carbon tab are positively deviated by anywhere from few % up to ~20% relative to the $^{235}U/^{238}U$, whereas for the UO_2 in epoxy, the $^{235}U^{16}O/^{238}U^{16}O$ uniformly displays better precision and accuracy despite the fact that trace amounts of carbon are present. However, the fact that several of the analyses on the sticky carbon tab produce $^{235}U^{16}O/^{238}U^{16}O$ with better precision and accuracy compared to the $^{235}U/^{238}U$ suggests that the process of forming the U-C molecular species is not consistent from analysis to analysis despite having an abundance of carbon available at the sputtering site. Furthermore, the effect of this interference would be expected to be far worse on the carbon sticky tab in comparison to the epoxy, even under circumstances where an uneven sample surface may have trapped some epoxy and/or abrasive particles during preparation. Therefore, it is not clear whether the carbon-based molecular interferences can serve as the sole explanation for why the compounds shown in Figures 5–8 exhibit highly scattered $^{235}U^{16}O/^{238}U^{16}O$ in comparison to their $^{235}U/^{238}U$ ratios.

Therefore, it is still worthwhile to consider additional origins for the highly unsTable $235U^{16}O/^{238}U^{16}O$ ratios displayed by some of the uranium compounds. In Figure 12, where the 1σ uncertainty of the $^{235}U^{16}O/^{238}U^{16}O$ relative to that of the $^{235}U/^{238}U$ ratios is plotted as a function of each analysis's average $^{238}U/^{238}U^{16}O$ ratio, there is a correlation between the results obtained from the $^{235}U^{16}O/^{238}U^{16}O$ versus the $^{235}U/^{238}U$ ratios and each analysis's average $^{238}U/^{238}U^{16}O$. More specifically, analyses with a higher average elemental oxide abundance trend toward $^{235}U^{16}O/^{238}U^{16}O$ ratios that are more precise than the $^{235}U/^{238}U$ ratios. This observation might favor the scavenging scenario described at the start of this section, because it could be used to state that analyses where there was less available oxygen ions to form the U-O molecular ion display poorer precision and accuracy in the $^{235}U^{16}O/^{238}U^{16}O$ ratio; however, this possibility is not supported by the fact that the two materials with the highest concentration of reactive ions and lowest uranium concentrations (the NIST 610 glass and the Plesovice zircon) align with the results from the UO_2, which is the only uranium compound not containing other elemental constituents.

Therefore, it is necessary to consider other reasons for worsening precision and accuracy at lower average uranium oxide molecular secondary ion formation rates. Another possibility that can be considered with the available data are the effects of topography. As discussed earlier regarding the potential for fluorine- and carbon-based molecular interferences, it is possible that carbon from the epoxy may have become trapped in the irregular surfaces of the some of the uranium compounds. However, it is also necessary to consider that topography can also have a direct effect on secondary ion yields [35].

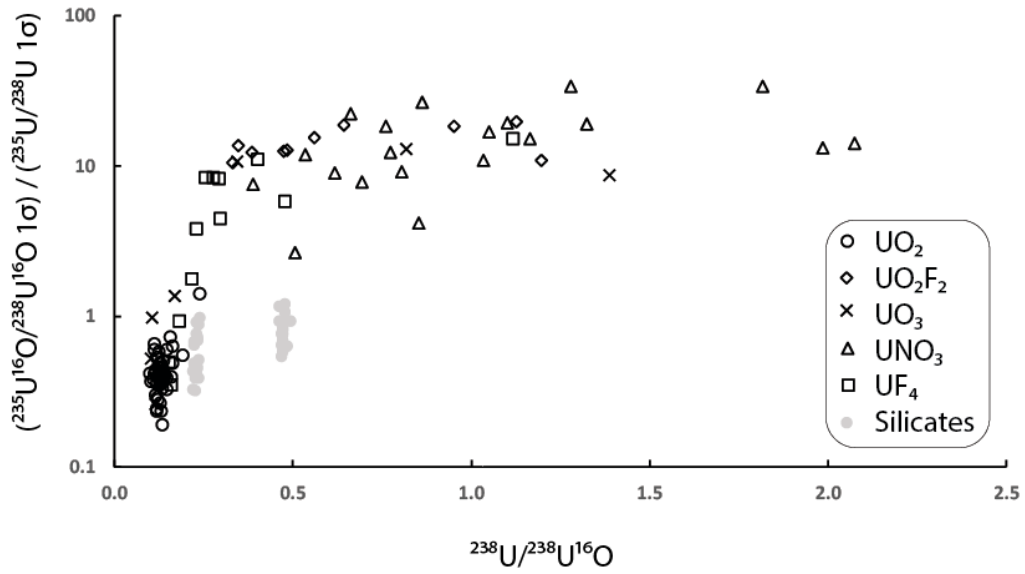

Figure 12. Plot of each analysis's uncertainty in the $^{235}U^{16}O/^{238}U^{16}O$ ratio relative to uncertainty in the $^{235}U/^{238}U$ ratio as a function of that analyses of average $^{238}U/^{238}U^{16}O$ ratio for the various uranium compounds and silicate materials examined in this study. Note the progression toward poorer precision of the $^{235}U^{16}O/^{238}U^{16}O$ relative to the $^{235}U/^{238}U$ ratio as the $^{238}U/^{238}U^{16}O$ ratio increases.

Examination of Figure 1 reveals that the UO_2 produced a flat surface when the mount was polished, whereas the UO_2F_2 did not. Although SEM images of the two silicate reference materials were not acquired as part of this study, both materials are routinely analyzed by SIMS and are known to produce highly polished and flat surfaces when mounted in epoxy and polished. While SEM images of the UO_3, $UO_2(NO_3)_2{\cdot}6(H_2O)$, and UF_4 are not shown, their surfaces are more similar to the UO_2F_2 than the nicely polished and flat surface of the UO_2. Therefore, another basic observation from the data is the uranium compounds with poor surface preparation produced considerably worse $^{235}U^{16}O/^{238}U^{16}O$ in comparison to the $^{235}U/^{238}U$ ratios. The effect of topography on the precision and accuracy of isotope ratios determined by SIMS has been investigated by several authors (see discussion by [35]), with the general consensus being that irregular surfaces can induce spot-to-spot variation at the per mil level. For the results of this study, it is important to note that the average levels of accuracy and precision associated with the $^{235}U/^{238}U$ ratios of the UO_2F_2, UO_3, $UO_2(NO_3)_2{\cdot}6(H_2O)$, and UF_4 are not considerably worse than for the UO_2. Rather, the difference is seen in the $^{235}U^{16}O/^{238}U^{16}O$ ratio. If sample topography is to blame for this behavior, then it would appear that the topographical influence on the $^{235}U^{16}O/^{238}U^{16}O$ is an order of magnitude greater than for the $^{235}U/^{238}U$.

It is possible that the irregular surface produced by mounting and polishing the UO_2F_2, UO_3, $UO_2(NO_3)_2{\cdot}6(H_2O)$, and UF_4 results in irregular UO^+ production, whereas the effect on the U^+ ions is not as drastic. This lack of consistency in the UO^+ production rate is evident in Figure 12, where it is clear that the materials for which use of the $^{235}U^{16}O/^{238}U^{16}O$ ratio resulted in improved precision and accuracy (the UO_2 and silicate reference materials) display a relatively narrow range in their $^{235}U/^{235}U^{16}O$ and $^{238}U/^{238}U^{16}O$ ratios. In contrast, the materials with highly variable average $^{235}U/^{235}U^{16}O$ and $^{238}U/^{238}U^{16}O$ secondary ion ratios between the different analyses have $^{235}U^{16}O/^{238}U^{16}O$ ratios with considerably poorer precision and accuracy in comparison to the $^{235}U/^{238}U$ ratios. While there may be other factors that contributed to this variability, the only readily observable difference between these materials and those that yielded more precise and accurate $^{235}U^{16}O/^{238}U^{16}O$ is the nature of the sample surface. Bulk chemistry or fluorine-based interferences may be factors, but the fact that the silicate reference materials yielded results such as the UO_2, as well as the results from the UO_2F_2 and UF_4, do not favor this possibility. For the individual analyses, whose $^{235}U^{16}O/^{238}U^{16}O$ ratios are biased high relative to the $^{235}U/^{238}U$ ratios, the effect of carbon-based interferences also cannot be

ruled out. However, comparison of results from UO_2 in epoxy versus UO_2 dispersed onto a sticky carbon tab suggest that the effect of the carbon-based interferences may not be adequate to account for the extreme deviances in the $^{235}U^{16}O/^{238}U^{16}O$ ratio displayed by some of the compounds. In the following section, the implications of these observations as well as a path to better understand this behavior are discussed.

4.4. Implications for SIMS Analysis and Need for Additional Studies

The results of this study indicate that use of the $^{235}U^{16}O/^{238}U^{16}O$ ratio can result in improved precision and accuracy for UO_2 during SIMS analysis, baring significant contribution to the $^{235}U^{16}O$ signal from $^{238}U^{13}C$. The most likely explanation for this effect is that the count rate of both the $^{235}U^{16}O^+$ and $^{238}U^{16}O^+$ consistently exceeds those of the $^{235}U^+$ and $^{238}U^+$ secondary ions by a factor of approximately 7.5 (Table S1). A similar effect is observed for the two silicate reference materials that were examined, even though the other uranium compounds examined exhibit less consistency (e.g., Figure 12). Therefore, in a situation where low count rates are an anticipated issue (e.g., a small amount of material is available or a high spatial resolution measurement with a low primary beam current is needed) and there is limited information about the chemistry of the material, a prudent approach would be to collect both the $^{235}U^{16}O^+$ and $^{238}U^{16}O^+$ molecular and $^{235}U^+$ and $^{238}U^+$ atomic secondary ions. Based on the data collected in this study, it should be readily apparent whether the $^{235}U^{16}O/^{238}U^{16}O$ or $^{235}U/^{238}U$ ratios will yield the result with the highest precision and accuracy. This is because the materials that displayed considerably diminished accuracy on the $^{235}U^{16}O/^{238}U^{16}O$ in comparison to the $^{235}U/^{238}U$ ratio also displayed considerably worse internal precision (as reflected by the higher 1σ values associated with each analysis). Therefore, based on the available data, choosing the ratio (e.g., $^{235}U/^{238}U$ versus $^{235}U^{16}O/^{238}U^{16}O$) with the highest precision should also result in selecting the most accurate ratios. However, there are several caveats that must be considered.

The $^{235}U/^{238}U$ and $^{235}U^{16}O/^{238}U^{16}O$ ratios reported in this study have not been corrected for any type of mass fractionation or other instrument specific bias. Therefore, it is not possible to evaluate which ratio (e.g., $^{235}U/^{238}U$ versus $^{235}U^{16}O/^{238}U^{16}O$) is most amenable to the type of correction regimes that are typically used in isotope ratio mass spectrometry. The basic conclusion outlined in the preceding section will likely apply to any type of correction regime that is applied, but a logical next step is to further study the behavior of the $^{235}U/^{238}U$ versus $^{235}U^{16}O/^{238}U^{16}O$ ratio in a suite of uranium compounds with certified uranium isotope compositions. During such an approach, it would also be worthwhile to determine whether the observations made in this study hold true at different $^{235}U/^{238}U$ ratios because all the materials examined in this study have depleted-to-natural $^{235}U/^{238}U$ ratios. Other important variables to test would be the effects of different sample surface morphologies and substrates, in addition to a systematic assessment of the potential interference contributions outlined in Section 4.3. In summary though, the basic observation that the raw $^{235}U/^{238}U$ and $^{235}U^{16}O/^{238}U^{16}O$ ratios are both quite close to the solution MC-ICP-MS results means that both ratios should be amenable to the application of a reference material-based correction scheme. Therefore, selection of the ratio with the lowest internal precision (e.g., 1σ value) should yield the 'best' result in count-rate-limited situations.

While this study was expressly focused on the $^{235}U/^{238}U$ determination, the possibility of taking advantage of the greater U-O molecular generation in comparison to the U elemental secondary ion production to improve accuracy and precision may also extend to other uranium isotope ratios. For example, the $^{236}U/^{238}U$ and $^{234}U/^{238}U$ ratios are important indicator of whether samples from a variety of matrices contain anthropogenically perturbed U (see discussion by [36–38]). Because the natural $^{234}U/^{238}U$ is ~0.000055, and $<10^{-10}$ for $^{236}U/^{238}U$ [37], the issue of low secondary ion count rates for ^{235}U that formed the basis of this investigation become much more severe for determination of the $^{234}U/^{238}U$ and $^{236}U/^{238}U$ by SIMS. Furthermore, the $^{236}U/^{238}U$ determination is compounded by the formation of $^{235}U^1H$ secondary ions (see discussion by [4]). While it is likely that the secondary ion count rates of the $^{236}U^{16}O$ (mass = 252.04077 amu) and $^{234}U^{16}O$ (mass = 250.035861 amu) molecular

species would exceed those of the ^{236}U and ^{234}U elemental secondary ions during SIMS analysis, MRPs (defined as M/ΔM) of 18,836.6 and 16,755.8 would be needed to separate interferences from $^{238}U^{14}N$ (mass = 252.053857 amu) and $^{238}U^{12}C$ (mass = 250.050783), respectively. Furthermore, examination of the mass scans provided as insets in Figure 12 reveals elevated secondary ion counts at masses ~250 and ~252, suggesting that a first step in exploring use of the elemental oxide ratios for the $^{236}U/^{238}U$ and $^{234}U/^{238}U$ determination would be to understand whether a suitable sample preparation route can be developed such that the contribution of nitrogen and carbon to the analytical volume is eliminated.

5. Conclusions

Comparison of the $^{235}U/^{238}U$ versus the $^{235}U^{16}O/^{238}U^{16}O$ ratios measured by NanoSIMS from a variety of uranium compounds and silicate reference materials indicate the following:

(1) For the UO_2 and silicate reference materials, which display internally consistent relationships between their UO^+ and U^+ secondary ion production rates, use of the $^{235}U^{16}O/^{238}U^{16}O$ ratio results in improved accuracy and precision compared to the $^{235}U/^{238}U$ ratio.

(2) For the UO_2F_2, UO_3, $UO_2(NO_3)_2{\cdot}6(H_2O)$, and UF_4, which have variable internal relationships between their UO^+ and U^+ secondary ion production rates, use of the $^{235}U^{16}O/^{238}U^{16}O$ ratio is associated with considerably worse accuracy and precision compared to the $^{235}U/^{238}U$ ratio.

(3) Preliminarily, the observed different behavior between the UO_2 and silicate reference materials versus the other uranium compounds appears attributable to the effects of sample topography, although the effects of fluorine- and carbon-based molecular interferences cannot be fully ruled out.

(4) Additional experiments are necessary to determine whether the observations made in this study can be applied to additional uranium compounds, other isotope compositions, different sample morphologies, and varied substrates.

Supplementary Materials: The following are available online at http://www.mdpi.com/2075-163X/9/5/307/s1, Table S1: NanoSIMS analytical results, Table S2: NanoSIMS mass scans.

Author Contributions: Conceptualization, N.A.Z.; methodology, N.A.Z., J.B.S., C.R.H., A.J.M., M.W.A.; formal analysis, N.A.Z., C.R.H., B.T.; investigation, N.A.Z.; resources, A.J.M.; writing—original draft preparation, N.A.Z., C.R.H.; writing—review and editing, J.B.S., A.J.M., D.C.D., B.W.T., M.W.A.; supervision, R.K.; project administration, R.K.; funding acquisition, R.K., N.A.Z., J.B.S.

Funding: Notice: This manuscript has been authored by UT-Battelle, LLC, under contract DE-AC05-00OR22725 with the US Department of Energy (DOE). The US government retains and the publisher, by accepting the article for publication, acknowledges that the US government retains a nonexclusive, paid-up, irrevocable, worldwide license to publish or reproduce the published form of this manuscript, or allow others to do so, for US government purposes. DOE will provide public access to these results of federally sponsored research in accordance with the DOE Public Access Plan (http://energy.gov/downloads/doe-public-access-plan). SEM analyses were conducted at the ORNL Center for Nanophase Materials Sciences, which is a DOE Office of Science user facility.

Acknowledgments: Constructive comments from three anonymous reviewers, and the editorial handling of Tony Simonetti, greatly improved the paper. Sarah Finkeldei and Lee D. Trowbridge, both of ORNL, are thanked for having provided a subset of the uranium compounds included in this study.

Conflicts of Interest: The authors declare no conflict of interest. The funders had no role in the design of the study; in the collection, analyses, or interpretation of data; in the writing of the manuscript, or in the decision to publish the results.

References

1. Tamborini, G.; Betti, M.; Forcina, V.; Hiernaut, T.; Giovannone, B.; Koch, L. Application of secondary ion mass spectrometry to the identification of single particles of uranium and their isotopic measurement. *Spectrochim. Acta Part B* **1998**, *53*, 1289–1302. [CrossRef]
2. Esaka, F.; Magara, M.; Lee, C.G.; Sakurai, S.; Usuda, S.; Shinodera, N. Comparison of ICP-MS and SIMS techniques for determining uranium isotope ratios in individual particles. *Talanta* **2009**, *78*, 290–294. [CrossRef] [PubMed]

3. Park, J.; Kim, T.H.; Lee, C.H.; Lee, J.; Lim, S.H.; Han, S.H.; Son, K. Combinatory use of time-of-flight secondary ion mass spectrometry (SIMS) and sector-field SIMS for estimating elemental and isotopic compositions of nuclear forensic samples. *J. Radioanal. Nucl. Chem.* **2017**, *311*, 1535–1544. [CrossRef]
4. Simons, D.S.; Fassett, J.D. Measurement of uranium-236 in particles by secondary ion mass spectrometry. *J. Anal. Atomic Spectrom.* **2017**, *32*, 393–401. [CrossRef]
5. Sharp, N.; Fassett, J.D.; Simons, D.S. Uranium ion yields from monodisperse uranium oxide particles. *J. Vac. Sci. Technol.* **2016**, *34*, 03H115. [CrossRef] [PubMed]
6. Zirakparvar, N.A.; Smith, J.B. *Commissioning Plan for the Cameca NanoSIMS 50L*; Oak Ridge National Laboratory: Oak Ridge, TN, USA, 2017.
7. Fitzsimons, I.C.W.; Harte, B.; Clark, R.M. SIMS stable isotope measurement: Counting statistics and analytical precision. *Miner. Mag.* **2000**, *64*, 59–84. [CrossRef]
8. Stern, R.A.; Bodorkos, S.; Kamo, S.L.; Hickman, A.H.; Corfu, F. Measurement of SIMS instrumental mass fractionation of Pb isotopes during Zircon dating. *Geostand. Geoanal. Res.* **2009**, *33*, 145–168. [CrossRef]
9. Eiler, J.M.; Graham, C.; Valley, J.W. SIMS analysis of oxygen isotopes: Matrix effects in complex minerals and glasses. *Chem. Geol.* **1997**, *138*, 221–244. [CrossRef]
10. Esaka, F.; Watanabe, K.; Onodera, T.; Lee, C.G.; Magara, M.; Sakurai, S.; Usuda, S. Dependence of the precision of uranium isotope ratio on particle diameter in individual particle analysis by SIM.S. *Appl. Surf. Sci.* **2008**, *255*, 1512–1515. [CrossRef]
11. Tenner, T.; Williamson, T.; Lamont, S. Particle Forensics: LANL Capabilities. Los Alamos National Laboratory document ID LA-UR-16-27896. Presented at the Nuclear Forensics Workshop, Livermore, CA, USA, 18 October 2016; Los Alamos National Laboratory: Los Alamos, NM, USA.
12. Hoppe, P.; Cohen, S.; Meibom, A. NanoSIMS: Technical aspects and applications in cosmochemistry and biological geochemistry. *Geostand. Geoanal. Res.* **2013**, *37*, 111–154. [CrossRef]
13. Ireland, T.R. Ion microprobe mass spectrometry: Techniques and applications in cosmochemistry, geochemistry, and geochronology. *Adv. Anal. Geochem.* **1995**, *2*, 1–118.
14. Kips, R.S.; Kristo, M.J. Investigation of chemical changes in uranium oxyfluoride particles using secondary ion mass spectrometry. *J. Radioanal. Nucl. Chem.* **2009**, *282*, 1031–1035. [CrossRef]
15. Ireland, T.R.; Williams, I.S. Considerations in zircon geochronology by SIM.S. *Rev. Mineral. Geochem.* **2003**, *53*, 215–241. [CrossRef]
16. Yang, W.; Lin, Y.T.; Zhang, J.C.; Hao, J.L.; Shen, W.J.; Hu, S. Precise micrometer-sized Pb–Pb and U–Pb dating with NanoSIM.S. *J. Anal. At. Spectrom.* **2012**, *27*, 479–487. [CrossRef]
17. Hunt, R.D.; Collins, J.L. Uranium kernel formation via internal gelation. *Radiochim. Acta* **2004**, *92*, 909–915. [CrossRef]
18. Miskowiec, A.; Kirkegaard, M.C.; Huq, A.; Mamontov, E.; Herwig, K.W.; Trowbridge, L.; Rondinone, A.; Anderson, B.B. Structural phase transitions and water dynamics in uranyl fluoride hydrates. *J. Phys. Chem. A* **2015**, *199*, 11900–11910. [CrossRef]
19. Geichman, J.R.; Smith, E.A.; Trond, S.S.; Ogle, P.R. Hexafluorides of molybdenum tungsten, uranium IReactions with nitrous nitric oxides. *Inorg. Chem.* **1962**, *1*, 661–665. [CrossRef]
20. Geichman, J.R.; Smith, E.A.; Ogle, P.R. Hexafluorides of molybdenum tungsten, uranium IIReactions with nitryl fluoride nitrosyl fluoride, nitrosyl chloride. *Inorg. Chem.* **1963**, *2*, 1012–1015. [CrossRef]
21. Zimmer, M.M.; Kinman, W.S.; Kara, A.H.; Steiner, R.E. Evaluation of the homogeneity of the uranium isotope composition of NISTSRM 610/612 by M.C.-I.C.P.-M.S, MC-TIMS and SIMS. *Minerals* **2014**, *4*, 541–552. [CrossRef]
22. Slama, J.; Kosler, J.; Condon, D.J.; Crowley, J.L.; Gerdes, A.; Hanchar, J.M.; Horstwood, M.S.A.; Morris, G.A.; Nasdala, L.; Norberg, N.; et al. Plešovice zircon—A new natural reference material for U–Pb and Hf isotopic microanalysis. *Chem. Geol.* **2008**, *249*, 1–35. [CrossRef]
23. Richter, S.; Eykens, R.; Kuhn, H.; Aregbe, Y.; Verbruggen, A.; Weyer, S. New average values for the n(238U)/n(235U) isotope ratios of natural uranium standards. *Int. J. Mass Spectrom.* **2010**, *295*, 94–97. [CrossRef]
24. Liu, M.C.; McKeegan, K.D.; Harrison, T.M.; Jarzebinksi, G.; Vltava, L. The Hyperion-II radio-frequency oxygen ion source on the UCLA ims1290 ion microprobe: Beam characterization and applications in geochemistry and cosmochemistry. *Int. J. Mass Spectrom.* **2018**, *424*, 1–9. [CrossRef]

25. Mahlerbe, J.; Penen, F.; Isaure, M.P.; Frank, J.; Hause, G.; Dobritzch, D.; Gontier, E.; Horreard, F.; Hillion, F.; Schaumloffel, D. A new radiofrequency plasma oxygen primary ion source on Nano Secondary Ion Mass Spectrometry for improved lateral resolution and detection of electropositive elements at single cell level. *Anal. Chem.* **2016**, *88*, 7130–7136. [CrossRef]
26. Andersen, C.A.; Hinthorne, J.R. Thermodynamic approach to the quantitative interpretation of sputtered ion mass spectra. *Anal. Chem.* **1973**, *45*, 1421–1438. [CrossRef]
27. Schroeer, J.M. Calculation from first principles of the yield of ions and excited neutral atoms sputtered from metal surfaces. *Surf. Sci.* **1973**, *35*, 485–486. [CrossRef]
28. Slodzian, G.; Lorin, J.C.; Havette, A. Isotopic effect on the ionization probabilities in secondary ion emission. *J. Phys.* **1980**, *41*, 555–558. [CrossRef]
29. Shimizu, N.; Hart, S.R. Isotope fractionation in secondary ion mass spectrometry. *J. Appl. Phys.* **1982**, *53*, 1303–1311. [CrossRef]
30. Harrison, D.E.J. Sputtering models–A synoptic view. *Radiat. Eff.* **1983**, *70*, 1–64. [CrossRef]
31. Gnaser, H.; Hutcheon, I.D. Significance of isotope effects for secondary-ion emission models. *Phys. Rev. B* **1988**, *38*, 11112–11117. [CrossRef]
32. Kinny, P.D.; Compston, W.; Williams, I.S. A reconnaissance ion-probe study of hafnium isotopes in zircon. *Geochim. Cosmochim. Acta* **1990**, *55*, 849–859. [CrossRef]
33. Jeon, H.; Whitehouse, M.J. A critical evaluation of U-Pb calibration schemes used in SIMS geochronology. *Geostand. Geoanal. Res.* **2015**, *39*, 443–452. [CrossRef]
34. Schaltegger, U.; Schmitt, A.K.; Horstwood, M.S.A. U-Th-Pb zircon geochronology by ID-TIM.S, SIM.S, and laser ablation ICP-MS: Recipes, interpretations, and opportunities. *Chem. Geol.* **2015**, *402*, 89–110. [CrossRef]
35. Kita, N.T.; Ushikubo, T.; Fu, B.; Valley, J.W. High precision SIMS oxygen isotope analysis and the effect of sample topography. *Chem. Geol.* **2009**, *264*, 43–57. [CrossRef]
36. Boulgya, S.F.; Heumann, K.G. Determination of extremely low 236U/238U isotope ratios in environmental samples by sector-field inductively coupled plasma mass spectrometry using high-efficiency sample introduction. *J. Environ. Radioact.* **2006**, *88*, 1–10. [CrossRef]
37. Xiao, G.; Jones, R.L.; Saunders, D.; Caldwell, K.L. Determination of $^{234}U/^{238}U$.; $^{235}U/^{238}U$ and $^{236}U/^{238}U$ Isotope Ratios in Urine Using Sector-Field Inductively Coupled Plasma Mass Spectrometry (SF-ICP-MS). *Radiat. Prot. Domsimetry* **2014**, *162*, 618–624. [CrossRef] [PubMed]
38. Gray, P.J.; Zhang, L.; Xu, H.; McDiarmid, M.; Squibb, K.; Centeno, J.A. Determination of $^{236}U/^{238}U$ and $^{235}U/^{238}U$ isotope ratios in human urine by inductively coupled plasma mass spectrometry. *Microchem. J.* **2012**, *105*, 94–105. [CrossRef]